Physics of Fluids

RESEARCH ARTICLE | MARCH 17 2025

Intrinsic thermoacoustic instability in hydrogen enriched partially premixed flames

Ankit D. Kumar (అంకిత్డికుమార్) ; James C. Massey ;
Preethi Rajendram Soundararajan (பிரீத்திஇராஜேந்திரம்சௌந்தரராஜன்) ; Isaac Boxx;
Nedunchezhian Swaminathan (நெடுஞ்செழியன்சுவாமிநாதன்)

Check for updates

Physics of Fluids 37, 034124 (2025)
https://doi.org/10.1063/5.0258444

View Online
Export Citation

Articles You May Be Interested In

LES-based prediction of technically premixed flame dynamics and comparison with perfectly premixed mode

Physics of Fluids (August 2022)

Influence of swirl intensity on combustion dynamics and emissions in an ammonia-enriched methane/air combustor

Physics of Fluids (March 2024)

Parametric instability in propagating flames and the impact of hydrogen enrichment on the onset of secondary instability

Physics of Fluids (October 2023)

09 April 2025 06:56:50

AIP Publishing

AIP Publishing
Physics of Fluids
Special Topics Open for Submissions
Learn More

Physics of Fluids ARTICLE pubs.aip.org/aip/pof

Intrinsic thermoacoustic instability in hydrogen enriched partially premixed flames

Cite as: Phys. Fluids **37**, 034124 (2025); doi: 10.1063/5.0258444
Submitted: 16 January 2025 · Accepted: 21 February 2025 ·
Published Online: 17 March 2025

View Online Export Citation CrossMark

Ankit D. Kumar (అంకిత్ డి కుమార్),[1,2,a] James C. Massey,[1,2]
Preethi Rajendram Soundararajan (பிரீத்தி இராஜேந்திரம் சௌந்தரராஜன்),[1] Isaac Boxx,[3]
and Nedunchezhian Swaminathan (நெடுஞ்செழியன் சுவாமிநாதன்)[1]

AFFILIATIONS

[1]Department of Engineering, University of Cambridge, Trumpington Street, Cambridge CB2 1PZ, United Kingdom
[2]Robinson College, University of Cambridge, Grange Road, Cambridge CB3 9AN, United Kingdom
[3]Chair of Optical Diagnostics in Energy, Chemical and Process Engineering, RWTH Aachen University, Aachen 52062, Germany

[a)]Author to whom correspondence should be addressed: adk46@cam.ac.uk

ABSTRACT

The influence of hydrogen addition on the intrinsic thermoacoustic instability in swirl stabilized partially premixed methane flames is investigated using large eddy simulation (LES) and reduced order modeling (ROM). The LES results compare well with the measurements. Hydrogen addition results in a significant deviation of the fundamental frequency from the cavity acoustic modes. The thermoacoustic behavior is analyzed using an ROM with the classical n–τ model for flame dynamics, where the interaction index n and time delay τ are deduced from the LES results. A parametric sweep of n and τ with ROM reveals a broad variation of the acoustic eigenvalues in the eigenspectrum. The eigenspectrum shows two distinct regions corresponding to the classical acoustic and intrinsic modes. These intrinsic modes are characterized by a distinct change in the sign of axial pressure gradient across the flame. In the hydrogen-enriched cases, the pressure mode shapes obtained from the ROM and LES analyses show this change in the axial pressure gradient across the flame zone. This is due to flame-induced *pulsation* dominating the near-field acoustics, resulting in the emergence of intrinsic modes. Further, general results obtained using the one-dimensional acoustic model on the influence of geometry on the stability of acoustic and intrinsic modes are discussed.

© 2025 Author(s). All article content, except where otherwise noted, is licensed under a Creative Commons Attribution (CC BY) license (https://creativecommons.org/licenses/by/4.0/). https://doi.org/10.1063/5.0258444

09 April 2025 06:56:50

I. INTRODUCTION

Hydrogen is gaining significant interest as a zero-carbon fuel to meet decarbonization goals. It is therefore important to explore blended hydrogen/hydrocarbon combustion as a first step toward decarbonization. Gas turbine (GT) combustors typically operate under fuel-lean conditions to reduce NOx emissions. Lean operation increases the risk of thermoacoustic instability, which results from the strong positive coupling between pressure fluctuations and heat release rate per unit volume.[1] These instabilities and resulting pressure oscillations can severely compromise the GT combustor's structural integrity. Although some past studies[2–5] have explored thermoacoustics of blended fuel combustion, there are several unanswered questions.

Recent studies have identified intrinsic thermoacoustic instability (ITA),[6–8] which is independent of acoustic reflections and distinct from the classical acoustic modes. Silva[9] has comprehensively reviewed ITA, and these instabilities must not be confused with Darrieus–Landau or thermodiffusive instabilities. In premixed flames, the intrinsic feedback loop is driven by velocity fluctuations producing heat release fluctuations. The upstream-traveling acoustic waves resulting from these heat release rate fluctuations lead to velocity perturbations in an upstream region, say burner mouth or swirler.[10] These velocity perturbations are then convected downstream toward the flame, completing the feedback loop. This instability does not strongly depend on acoustic reflections and does not always produce heat release rate fluctuations, with frequencies close to that of cavity modes.

Intrinsic thermoacoustic instabilities can occur even when acoustic reflections are present. Both acoustic and intrinsic modes can coexist if there are reflections and intrinsic feedback loops. Partial premixing can create an intrinsic feedback loop driven by equivalence ratio perturbations. Differences in the acoustic impedance for air and fuel streams produce mixture inhomogeneities, which are convected downstream and influence the flame response. The resulting upstream-traveling acoustic waves modulate the air and fuel streams producing equivalence ratio perturbations, which close the feedback

© Author(s) 2025

loop. This loop is intrinsic because it operates independently of acoustic reflections, and its characteristic frequency in anechoic conditions depends only on the time delay. Several studies[3,11–14] have identified the equivalence ratio driven feedback loop in the PRECCINSTA burner that is considered for this study, and the individual contribution of equivalence ratio and velocity driven flame response were also investigated.[4,15] However, the aspects of intrinsic modes were not studied.

Passive control measures can destabilize ITA modes while stabilizing acoustic modes.[16] Therefore, classifying thermoacoustic modes as intrinsic and acoustic is required to develop tailored control measures for them. The flame transfer function (FTF) has a phase of $-\pi$ for ITA frequencies in anechoic systems, which led to the "π" criterion described by Hoeijmakers *et al.*[6] However, achieving an unambiguous distinction between acoustic and intrinsic modes in a non-anechoic system is challenging. A recently proposed criterion, known as a phasor criterion, suggests that the thermoacoustic mode is intrinsic if the velocity phase jump across the flame is between $\pi/2$ and π and acoustic if the phase jump is less than $\pi/2$.[17,18] This criterion was proposed for an ideal resonator of constant area. However, an area change can lead to ITA mode frequencies, which are significantly different from those suggested by the "π" criterion.[19] The extended criterion of Albayrak *et al.*[19] assumed nonreflecting (anechoic) boundaries, whereas the phasor criterion is not limited only to anechoic boundaries. The area change effects on ITA modes have been previously studied[8,9] but were limited to anechoic conditions[8] or special cases such as vanishing gain limit and neutrally stable cases.[9] Hence, a comprehensive study on these effects is lacking. Furthermore, the range of relevant parameters exciting the intrinsic or acoustic modes is yet to be determined.

To date, only one numerical study[20] on ITA modes in laminar slit flames used blended methane/hydrogen mixtures, which showed that adding hydrogen suppresses this mode. Therefore, it is natural to ask whether these observations apply for systems of practical interest. This question is addressed here along with the following specific objectives: (i) to investigate the emergence of ITA feedback in a partially premixed swirl combustor and the hydrogen addition effects on this feedback and (ii) to understand the effects of area change on ITA modes in multi-cavity systems. These objectives are addressed using pressure measurements, Large eddy simulations (LESs), Reduced Order Modeling (ROM), and a one-dimensional (1D) acoustic model. The pressure measurements and LES results form the basis for hypothesizing a possible intrinsic feedback in the cases investigated. This hypothesis is confirmed using ROM by evaluating the eigenspectrum and spatial characteristics of the modes in the geometry studied. The ROM is employed solely for these purposes, and a non-linear analysis is beyond the scope of this work. Additionally, a multi-cavity 1D acoustic model is used to draw general conclusions about the effects of area change on intrinsic modes.

This paper is organized as follows. The theoretical background is presented in Sec. II. The LES modeling methodology and the experimental setup are briefly outlined in Sec. III. The experimental, LES, ROM, and 1D acoustic model results are discussed in Sec. IV, and the conclusions are summarized in Sec. V.

II. BACKGROUND

Neglecting mean flow effects, the thermoacoustic instability in low Mach number flows is represented well using the inhomogeneous Helmholtz equation, and this equation in the frequency space is written as

$$\nabla \cdot \left(\bar{c}^2 \nabla \hat{p}\right) + s_k^2 \hat{p} = -i s_k (\gamma - 1)\hat{\dot{Q}}, \tag{1}$$

where $\bar{c}$ is the mean speed of sound, s_k is the k-th eigenmode, γ is the ratio of the specific heat capacities, and $i = \sqrt{-1}$. The quantities $\hat{p}$ and $\hat{\dot{Q}}$ are Fourier-transformed pressure and volume-integrated heat release rate fluctuations, respectively. The flame response is often related to the velocity fluctuations at a reference location $\mathbf{z}_{\text{ref}}$ (see Fig. 1) using the familiar n–τ model:[21]

$$\hat{\dot{Q}} = n \exp(-i s_k \tau) \nabla \hat{p}|_{\mathbf{z}_{\text{ref}}} \cdot \hat{\mathbf{j}}_{\mathbf{z}_{\text{ref}}}, \tag{2}$$

where n is the interaction index, τ is the time delay, and $\hat{\mathbf{j}}_{\mathbf{z}_{\text{ref}}}$ is the unit vector in the axial direction at $\mathbf{z}_{\text{ref}}$. Equations (1) and (2) constitute an eigenvalue problem whose solution gives a complex-valued eigenpair, which is composed of eigenmodes and eigenvalues $s_k \equiv \omega_k - i\sigma_k$ (for the ansatz $\hat{p} \sim \exp(i s_k t)$) where the real part of the eigenvalue corresponds to the angular frequency ($\omega_k = 2\pi f_k$) and the imaginary part ($\sigma_k = 2\pi g_k$) is the angular growth rate.

The ITA modes were originally identified in anechoic conditions,[6] but the distinction between acoustic and intrinsic modes in non-anechoic conditions was made only using a parametric study.[22,23] For instance, within the framework of the classical n–τ model, Orchini *et al.*[22] defined a mode characterization based on an asymptotic ($n \to 0$) behavior of the eigenvalues of Eq. (1). The coupling strength between flame and acoustics was also used in a past study[10] to discern ITA or acoustic modes. As $n \to 0$, two scenarios arise: (i)$\lim_{n\to 0} |n \exp(-i s_k \tau)| \to 0$ for a finite ω_k, which corresponds to a pure acoustic mode in the absence of a flame and (ii) $\lim_{n\to 0} |n \exp(-i s_k \tau)| \to \mathcal{O}(1)$ as $\sigma_k \to \infty$, which corresponds to an infinitely damped pure ITA mode. As $n \to 0$, the pure ITA mode has non-negligible contributions of $\mathcal{O}(1)$ from the flame. Reflection coefficients, R, at the boundaries were varied in past studies to recognize this mode as $R \to 0$.[10,24]

Performing parametric sweeps is not always practically feasible, and parameters like n and τ may not always have a one-to-one correspondence with physically controllable parameters in combustion systems. A physically intuitive criterion using the phase difference of

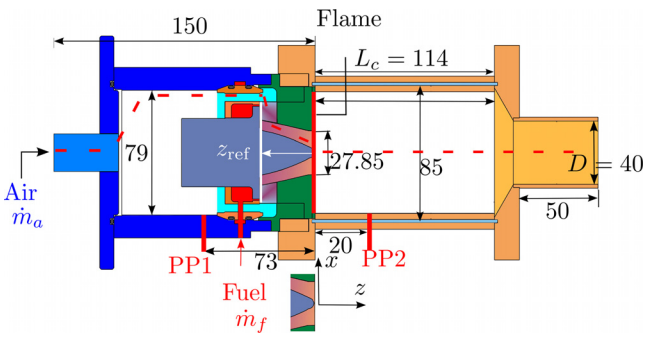

FIG. 1. Schematic of the gas turbine model combustor showing locations of the pressure probes PP1 (LES) and PP2 (LES, Exp). The flame is acoustically compact (shown using a red solid line for ROM) and is assumed to be located at the dump plane. The path used to evaluate the mode shape in the ROM is shown as a red dashed line.

09 April 2025 06:56:50

© Author(s) 2025

acoustic velocity across the flame was proposed by Yong *et al.*[18] This is called as *phasor criterion*, where the phasor represents the axial velocity as a complex vector in a cylindrical coordinate system. At each axial location of the phasor, the azimuthal and radial coordinates represent the phase and amplitude of the axial velocity. In this work, the phasor is considered only at the flame location and the discussion is restricted to only longitudinal (axial) modes. According to this criterion,[18] a pure intrinsic mode has a velocity phase jump of π across the flame, while a pure acoustic mode (no flame) has no velocity phase jump. In a standing acoustic mode, the velocity antinodes oscillate in phase, indicating that the fluid across the flame (ignoring the mean flow) *swings* back and forth in phase, i.e., in the same direction. It is worth noting that the fluid motion caused by acoustic waves is unidirectional since only axial modes are considered. The flow becomes incoherent and three-dimensional with turbulence. However, the focus is only on coherent and unidirectional flow caused by acoustic perturbations for this study. In contrast to a standing acoustic mode, the fluid on either side of upstream and downstream of the flame moves in opposite directions or *pulsates* when there is an intrinsic mode.[18] A general thermoacoustic mode may experience a velocity phase jump, φ_{ud}, spanning the entire range between 0 and π, and therefore, a mode is categorized as acoustic if $0 \leq \varphi_{ud} < \pi/2$ and intrinsic if $\pi/2 \leq \varphi_{ud} \leq \pi$. In general, the motion of the fluid medium with thermoacoustic instabilities can be described as a combination of the *swinging* and *pulsating* motions. The mode is characterized as intrinsic if the pulsating motion arising from fluctuating dilatation dominates over the swinging motion and *vice versa*.

III. LES MODELING METHODOLOGY AND EXPERIMENTAL SETUP

Fully compressible Favre-filtered transport equations for mass, momentum, and total enthalpy are solved. A presumed joint probability density function (PDF) approach with tabulated chemistry is used to model the filtered reaction rate.[25–27] The mixture fraction ξ, which tracks fuel-air mixing, is defined using Bilger's formula.[28] The progress variable, which represents the extent of reaction, is defined as $c = \psi/\psi^{eq}$, where $\psi = Y_{CO} + Y_{CO_2}$, and ψ^{eq} represents the equilibrium value for the local mixture fraction.[25–27] Thermochemical quantities are functions of $\tilde{\xi}$, $\tilde{c}$, and their respective sub-grid scale (SGS) variances. These four control variables and the total enthalpy are obtained from their transport equations described in Refs. 5,26,27,29. Further modeling and their validation for hydrogen enriched combustion are given in Ref. 5. All walls are assumed to be adiabatic. A constant mass flow rate is specified at the inlet, implying that there is no velocity fluctuation at the inlet. A hemispherical domain with a wave-transmissive boundary condition on the curved surface is included at the combustor exit to mimic the realistic room conditions.

Figure 1 shows the schematic of the PRECCINSTA combustor[30] used for this study. Dry air at ambient conditions enters the burner nozzle through 12 radial swirl channels after passing through a plenum. The fuel plenum is included in the computational model following an earlier study.[31] This plenum feeds fuel into the air stream through orifices located within each of the 12 radial swirl channels. The conical central body in the convergent nozzle with an exit diameter of 27.85 mm has its tip located at the nozzle exit plane (dump plane). Further details of the experimental setup can be found in Refs. 2 and 30. The operating conditions of the cases studied here are listed in Table I. The acoustic wave propagation in this PRECCINSTA burner is approximated using a 1D four-cavity (plenum, injection tube, combustion chamber, and exit tube) model to be discussed in Sec. IV C. Although all four cavities are modeled, it is referred to as a "3-cavity model" following the common terminology where the exit tube is typically included with the combustion chamber.

IV. RESULTS AND DISCUSSION

First, LES results are presented and compared to the measurements. Subsequently, the results from ROM are presented, followed by a general discussion on a 3-cavity acoustic model for the PRECCINSTA burner. The LES and experimental results offer reason to surmise the presence of an ITA mode. This is confirmed using ROM discussed in subsection IV B. Furthermore, the analysis using 3-cavity model extends the past work,[18] offering insights and guidelines to mitigate ITA modes that are not specific to the PRECCINSTA burner.

A. Thermoacoustic spectra

Figure 2 shows the pressure and heat release rate spectra from LES for the cases listed in Table I along with the measured pressure spectra. The computed pressure spectra (at probe PP2) and volume-integrated heat release rate spectra exhibit peaks around 300, 370, and 390 Hz for cases H0, H20, and H50, respectively. In contrast, the measured spectra show peaks at approximately 220, 283, and 415 Hz. These modes correspond to the plenum mode with the peak pressure amplitude occurring in the plenum. Case H20 displays two dominant peaks in both the computed (around 370 and 550 Hz) and measured pressure spectra (around 283 and 568 Hz), which is associated with a period-2 thermoacoustic oscillation involving interactions between plenum and combustion chamber modes as discussed by Kumar *et al.*[5,29]

The quartz windows used for optical access are loosely fitted to avoid their breakage during the limit-cycle oscillation. This results in some structural damping, which is extremely challenging to characterize and replicate in computational simulations. Therefore, some differences in the thermoacoustic amplitude are seen in Fig. 2, which are typical for this combustor.[14] The adiabatic boundary conditions used for LES lead to significant flame flashback,[5] which yields an overestimate in the fundamental frequencies for cases H0 and H20. However, this comparison is improved for H50 case since significant flame flashback occurs even in the experiments.[2] Alternative thermal boundary conditions, such as isothermal walls, heat resistance tuning (HRT), or conjugate heat transfer (CHT),[12,32] will merely improve results without affecting the main conclusions. However, these alternative thermal boundary conditions result in numerical challenges[33] and uncertainties related to modeling natural convection outside the combustor. For

TABLE I. Operating conditions for the cases studied, where ϕ_{glob} is the global equivalence ratio, $\%H_2$ (vol.) is the H_2 volume percentage in the fuel, P_{th} is the thermal power, and the mass flow rates of fuel and air are $\dot{m}_f$ and $\dot{m}_a$, respectively.

Case	ϕ_{glob}	$\dot{m}_f$ (g/s)	$\dot{m}_a$ (g/s)	$\%H_2$ (vol.)	P_{th} (kW)
H0	0.65	0.40	10.55	0	20
H20	0.65	0.38	10.43	20	20
H50	0.65	0.35	10.14	50	20

09 April 2025 06:56:50

© Author(s) 2025

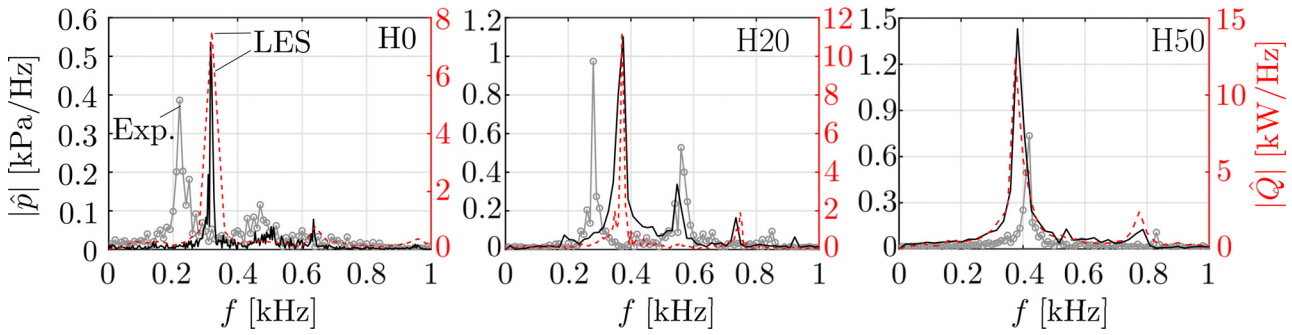

FIG. 2. The spectrum of $\hat{p}$, which are obtained from pressure fluctuations at probes PP2 (see Fig. 1) and $\dot{\hat{Q}}$. The gray and solid black lines are measured and computed (LES) pressure spectra, respectively. The computed spectra of $\dot{Q}$ are shown using red dashed lines.

simplicity, this work adopts the adiabatic boundary condition outlined in a previous study that uses the same LES modeling methodology.[5]

The thermoacoustic feedback loop in cases H0 and H20 is driven by velocity and equivalence ratio perturbations,[5] as typically seen in the PRECCINSTA burner for different operating conditions.[11,14,30] The timescale of the equivalence ratio driven feedback loop and hence its frequency depends on three important physical processes each with its own timescale, which are a convective timescale τ_{conv}, a consumption timescale τ_c, and an acoustic timescale τ_a.[5] First, the equivalence ratio perturbation is convected toward the flame with a timescale τ_{conv}. Second, the mixture inhomogeneities interact with the flame and are consumed over the span of τ_c. Third, the consumption of these inhomogeneous mixtures produces additional dilatation, which produce acoustic waves some of which travel toward the fuel nozzle over a span of τ_a. Addition of hydrogen substantially decreases τ_c, whereas τ_{conv} and τ_a change negligibly,[5] resulting in the observed increase in frequency.

The equivalence ratio-driven feedback loop is independent of the acoustic reflections. Furthermore, the substantial deviation of the fundamental frequency from the cavity mode (at about 280 Hz as shown in Fig. 3) is one of the defining characteristics of the intrinsic mode.[9] The change in the cavity mode frequency with H_2 addition is negligible since the sound speed changes marginally (not shown) across these cases. Further to the above feedback loop, the classical loop resulting from the acoustic reflections from boundaries may also be present.

In the following subsections, additional analysis is presented to ascertain the nature of these modes, specifically to confirm if they are ITA modes and to gather more general insights on them using an idealized 3-cavity system.

B. Reduced order model (ROM)

An open source 3D Helmholtz solver JULHOLTZ[22] is used to estimate the system stability and to characterize the unstable modes using their mode shapes. The thermoacoustic modes are obtained from the solution of Eqs. (1) and (2) in the computational domain used for LES,[5,29] but this domain is discretized using 70 000 tetrahedral cells for the ROM. In this domain, the hot gases are exhausted into a hemispherical volume mimicking the exterior domain. The mean sound speed field obtained from the LES is specified for the ROM. The eigenvalues of Eqs. (1) and (2) are obtained using the JULHOLTZ solver[22] for a range of n–τ values, with a closed–open acoustic boundary condition similar to the LES. The eigenvalues are evaluated using Beyn's contour integration method,[34] since fixed point algorithms fail to converge to ITA eigenvalues, especially close to the exceptional point (EP), which is a branch point singularity. The flame is assumed to be acoustically compact and is located at the dump plane. The classical closed–open acoustic boundary conditions are used where the inlet is specified with $\nabla\hat{p} = 0$ and the outlet (hemispherical surface of the exterior volume) is specified with $\hat{p} = 0$.

1. General assumptions

Since the complete non-linear behavior is not the focus here, the n–τ model is employed following its successful use in the past.[35] Flame transfer functions (FTFs) and reflection coefficients are not available from the experiments at these operating conditions. Hybrid LES/system identification (SI) techniques[36] have to be employed in either an incompressible or compressible framework with Characteristics-Based State-space Boundary Conditions (CBSBC)[37] to obtain FTFs with minimal bias,[36] which is beyond the scope of this work. However, it is possible to utilize the n–τ model in an approximate sense to characterize and better understand the observed modes. The following assumptions are made for the ROM:

i. Estimation of interaction index n: For the flame considered in this study, heat release rate oscillations arise due to both velocity fluctuations and mixture fracture fluctuations. The effects of both these fluctuations are considered in a combined manner[4,15] using an interaction index n defined as

$$n \approx \frac{|\hat{\dot{Q}}|/\overline{\dot{Q}}}{|\hat{\mathbf{u}}|/\langle\overline{\mathbf{u}}\rangle}, \tag{3}$$

where $|\hat{\dot{Q}}|$ and $|\hat{u}|$ are the amplitudes of the Fourier transformed volume-integrated heat release rate fluctuation and velocity fluctuation at the dump plane. The corresponding time-averaged quantities at the dump plane are denoted using $\overline{Q}$ and $\langle\overline{u}\rangle$, respectively. The velocity at the dump plane is decomposed as $\mathbf{u}(t) = \langle\overline{\mathbf{u}}\rangle + \mathbf{u}'(t)$, where $\mathbf{u}'(t)$ is the velocity fluctuation. All quantities required for the evaluation of n in Eq. (3) are obtained from the LES after the limit cycle oscillation is reached. The interaction index (or gain) is typically obtained by forcing the flame acoustically at different frequencies, which suitably represents the flame behavior under self-excited oscillations.[38,39] In

09 April 2025 06:56:50

© Author(s) 2025

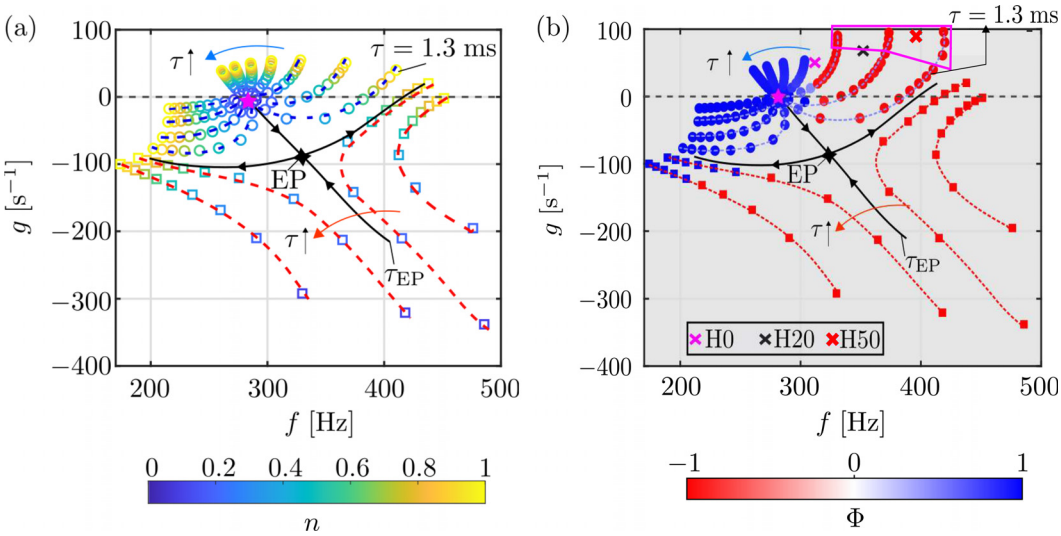

FIG. 3. (a) Eigenvalue trajectories for $n \in [0, 1]$ and $\tau \in [0, 3]$ ms. Circles and squares denote eigenvalues of the acoustic and intrinsic origins based on the asymptotic criterion. The blue and red dotted line trajectories demarcate the trajectories of acoustic and intrinsic modes based on this criterion, respectively. The black diamond denotes an EP. The black solid lines denote isolines of $\tau_{EP} = 1.223$ ms. The pink star denotes the pure acoustic plenum mode. Blue and red arrows show the direction of increasing τ for acoustic and intrinsic modes, respectively. (b) Same as in (a), except that the points are colored to denote the acoustic (blue) or ITA (red) modes using the phasor criterion with $\Phi = \cos(\varphi_{ud})$. Three colored crosses denote the eigenvalues corresponding to the LES cases. Additional ITA eigenvalues for $\tau = 1.3, 1.5$, and 1.8 ms and $n = 1.2, 1.4$, and 1.6 are marked within the pink colored pentagon.

this work, the interaction index is extracted from a self-excited case at the specific frequencies of instability similar to a previous work.[38] In addition, the velocity in Eq. (3) is calculated at the dump plane since the fluctuations at this location are in the immediate vicinity of the flame. This location is different from $\mathbf{z}_{ref}$ discussed next.

ii. Estimation of time-delay τ: The time-delay τ is the delay between $\dot{Q}'$ and velocity fluctuations $\mathbf{u}'_{\mathbf{z}_{ref}}$ at $\mathbf{z}_{ref}$, which is chosen to be the plane at which fuel enters the swirler. The axial distance between the $\mathbf{z}_{ref}$ and the dump plane is small (compared to the acoustic wavelength) and that the velocity magnitude is not very different between the two locations. This choice is based on earlier studies[3,5,11,40] showing that the thermoacoustic instability is driven by mixture fraction fluctuations generated at the fuel injection point. Similar choices for $\mathbf{z}_{ref}$ were made in the past.[40] To minimize the modeling effort, the dump plane is taken as the reference location while evaluating n to eliminate the need for a convective–diffusive model.

iii. Mean flow effects: The mean flow has at least three physical effects: (i) Convection of perturbations in a mixture fraction and vorticity resulting in delayed flame response, (ii) acoustic pressure losses due to fluid acceleration across area change, and (iii) change in wave propagation speed. The first effect is already considered in the n–τ model where a part of the time delay constitutes delay due to convection. The second effect is usually $\mathcal{O}(M^2)$, and since the maximum mean Mach number M is very low (about 0.04), it is neglected along with the third effect.

iv. Thin flame assumption: The flame is assumed to be acoustically compact,[22,35] which is justified since the flame length ($l_f \approx 0.06$ m) is an order of magnitude lower than the lowest wavelength in case H50 ($\overline{c_u}/f_1 \approx 0.87$ m). The speed of sound in the unburnt gas ($\overline{c_u}$) is considered since f_1 corresponds to the plenum mode and the fluid medium in the plenum is mostly cold air. The chamber mode at frequency f_2, which is excited in case H20 corresponds to a higher wavelength ($\overline{c_b}/f_2 \approx 1.52$ m).

v. Acoustic boundary conditions: The mass flow rate is held constant at the inlet for the LES and experiments, and hence the inlet is treated as a velocity node ($\hat{u} = 0$ and $\nabla\hat{p} = 0$, where $\hat{u}$ is the Fourier-transformed acoustic velocity). The pressure fluctuations at the outlet (surface of the hemispherical volume) are negligible, and hence a pressure node is assumed on this surface ($\hat{p} = 0$).

2. Eigenspectrum

The eigenvalue trajectories obtained by varying n and τ are shown in Fig. 3(a), where each marker denotes a specific eigenvalue. The variation seen in the figure is similar to the past work[22] and includes two distinct trajectories of acoustic (blue dashed lines) and intrinsic (red dashed lines) origins on which a collection of discrete eigenvalues are marked using circles (acoustic) or squares (intrinsic). The categorization between acoustic and intrinsic modes in Fig. 3(a) is made using the asymptotic criterion of Orchini *et al.*[22] There is a strong mode veering close to the region where the red and blue-colored trajectories approach the black diamond, which marks the EP. At an EP, the acoustic and ITA modes coalesce and their identity can be associated with neither of them. The interested reader may find more details about the properties of EPs in Ref[41] and about their relevance to thermoacoustic systems in a recent review by Silva[9]

Figure 3(b) is similar to Fig. 3(a) with three differences. First, the discrete eigenvalue markers are colored using $\Phi = \cos(\varphi_{ud})$. Second, there are three cross markers for the eigenvalues with n and τ values inferred from LES cases listed in Table II. The n and τ values are

09 April 2025 06:56:50

© Author(s) 2025

TABLE II. List of thermoacoustic parameters, frequencies, and growth rates from LES and ROM ($f_1 = \omega_1/2\pi$ and $g_1 = \sigma_1/2\pi$).

Case	n	τ (ms)	f_{LES} (Hz)	f_1 (Hz)	g_1 (s^{-1})
H0	0.85	1.90	300	318	+47.92
H20	1.45	1.60	370	356	+76.38
H50	1.5	1.40	390	393	+83.40

determined by procedures discussed in Section IV B1. Third, three additional intrinsic eigenvalues (in red) are marked for $n = 1.2$, 1.4, and 1.6 along trajectories closest to the LES cases, and these eigenvalues are enclosed by a pink colored pentagon in Fig. 3(b). These trajectories begin as acoustic modes at low n values, and transition to an intrinsic mode as n increases (see $\tau = 1.3$ ms trajectory as an example). Figure 3(a) does not capture this transition, and all eigenvalues along the $\tau = 1.3$ ms trajectory are acoustic modes. It is therefore physically meaningful to use the phasor criterion because it captures the mode transition. Based on this criterion, the eigenvalues inferred from LES appear in the ITA region, with the case having the lowest hydrogen content (H0) closest to the acoustic region. Additionally, n increases and τ decreases upon hydrogen addition similar to a recent study on the same burner at a different operating condition.[4] Therefore, in this case, hydrogen addition results in the destabilization of ITA, unlike the findings of Ghani and Polifke[20] where intrinsic modes were stabilized by H_2 addition.

Figure 4 shows the pressure mode shape for two extreme cases, namely, pure acoustic mode and a pure (infinitely damped) ITA mode. The pressure mode shape is the normalized amplitude of the fundamental mode expressed as a function of the axial coordinate and is evaluated along the path shown in Fig. 1. It is clearly seen that the pure acoustic mode has the highest amplitude in the plenum ($z/L_c < 0$, where L_c is the combustor length as shown in Fig. 1), whereas the pure ITA mode peaks in the vicinity of the flame. The pure ITA mode shape also shows a change in axial pressure gradient, which is consistent with the phasor criterion. This is straightforward to

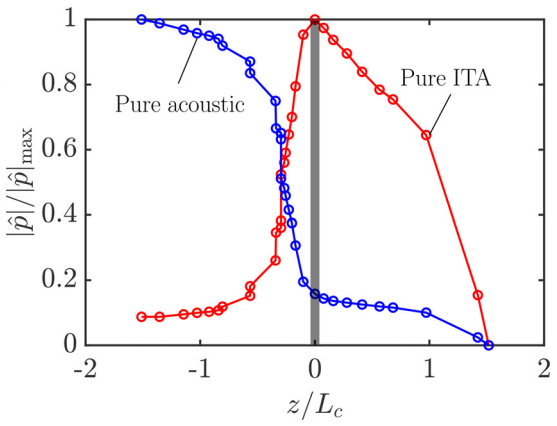

FIG. 4. Mode shapes of pure acoustic mode (blue) and pure ITA mode (red) obtained using ROM from discrete points along the path shown in Fig. 1. The thick gray line marks the position of the flame. The results are chosen for arbitrary chosen $n = 0.01$ and $\tau = 1.3$ ms.

see by rewriting the first-order perturbed momentum equation (neglecting convection and viscous terms) in frequency space as[17]

$$is_k\hat{u} \approx \frac{-1}{\overline{\rho}}\nabla\hat{p}, \tag{4}$$

where $\overline{\rho}$ is the time-averaged density. Equation (4) shows that a change in the sign of $\hat{u}$, which occurs for ITA mode ($\varphi_{ud} > \pi/2$), results in the change in the pressure gradient sign. Therefore, all eigenvalues indicated with red markers in Fig. 3(b) have a change of sign in the axial pressure gradient across the flame, as seen in Fig. 4 for the ITA mode.

This aspect is further exemplified in Fig. 5(a) showing the mode shapes for the fundamental frequency. The results are obtained from the LES and ROM. Also, the corresponding experimental measurements at the PP2 location are shown for comparison. The mode shape in the upstream side of the flame located at $z/L_c = 0$ for the H0 case is similar to the pure acoustic mode shape shown in Fig. 4. The axial pressure gradient increases across the flame before decreasing downstream of the flow as seen in Fig. 5(a). The mode shape in the plenum ($z/L_c < 0$) does not change with the addition of H_2, but the shape and axial pressure gradient near the flame change drastically as shown in Fig. 5(a) for the H20 and H50 cases. These features are also captured by the ROM as seen in Fig. 5(a). The LES results marked in Fig. 3(b) clearly show that the eigenvalues move deeper into the intrinsic region as the hydrogen content is increased. Therefore, the addition of hydrogen increases the flame induced *pulsation* resulting in the ITA modes in the configuration studied here.

Figure 5(b) shows the axial variation of velocity phase for the 3 cases as obtained from the LES and ROM. The phase difference of the cases is greater than $\pi/2$, which offers evidence for the presence of ITA modes in these cases. The corresponding $\Phi = \cos(\varphi_{ud})$ values obtained from the ROM for the three cases are −0.20 (H0), −0.51 (H20), and −0.72 (H50), clearly suggesting an increase in the phase difference (φ_{ud}) with hydrogen addition. The ROM captures the phase variations well and is in good comparison with the LES albeit with some differences. The discrepancies between LES and ROM may arise from the linear n–τ model chosen for ROM. These analyses clearly identified the presence of ITA modes in the cases studied here.

While the results discussed above are specific to the PRECCINSTA burner, a general 3-cavity acoustic model is studied in the next section to understand the area ratio effects on the stability of ITA modes. These results are fairly general and offer guidelines to mitigate both ITA and acoustic modes, if required.

C. A 3-cavity acoustic model

This section discusses a 1D acoustic model for a 3-cavity geometry with area change typically seen in combustion systems. The schematic of this model, resembling the PRECCINSTA burner, is shown in Fig. 6. The three cavities represent the plenum (section $j = 0$), an injection unit with a swirler (section $j = 1$), and a combustion chamber along with the exit tube (section $j = 2$ and $j = 3$). The combustion chamber and the exit tube, taken together, are semantically treated as the third cavity while still considering the different lengths and areas (l_2, l_3, S_2, and S_3). The plenum, injector, and exit tube of the PRECCINSTA burner have a circular cross section, while the combustor has a square section. The radius of section $j = 3$ is $r_3 = 20$ mm, and section $j = 2$ has a cross-sectional area of 85×85 mm^2. The effect

09 April 2025 06:56:50

© Author(s) 2025

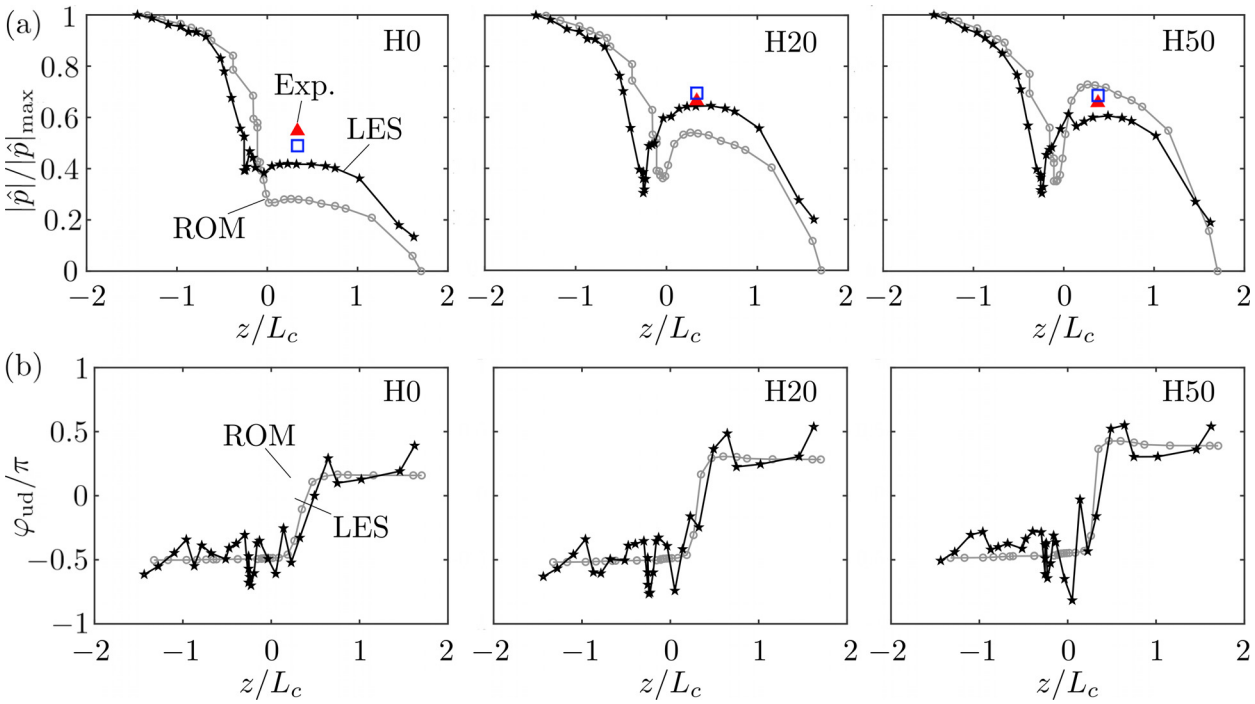

FIG. 5. Axial variation of (a) the pressure amplitude and (b) velocity phase obtained from ROM and LES for cases H0, H20, and H50. The ratio of the pressure amplitude at probe PP2 to probe PP1 from LES (blue square) and experiments (red triangle) are also shown in the top row for PP2 location (see Fig. 1). The flame is positioned at $z/L_c = 0$.

of the area jump across the plenum and the injection tube is studied by varying either r_0 or r_1, where r_1 takes the values 38.00, 27.63, and 21.71 mm and r_2 takes the values 8, 11, and 14 mm. Section $j = 1$ is approximated as a constant area tube for simplicity, and the true value for the PRECCINSTA lies in the ballpark of the chosen values. The unburnt gas mixture in the plenum and the injection unit is at a temperature $\overline{T_u} = 298$ K and has a density of $\overline{\rho_u} = 1.225\,\mathrm{kg/m^3}$. The speed of sound in this mixture is $\overline{c_u} = \sqrt{\gamma R \overline{T_u}}$, where $R = 287.1\,\mathrm{J/kg/K}$ is the specific gas constant and $\gamma = 1.4$ is the ratio of the specific heat capacities at constant pressure and volume. The burnt gas mixture in the combustion chamber is at a temperature $\overline{T_b} = 1850$ K, density $\overline{\rho_b} = (p_0/R\overline{T_b})$, where $p_0 = 101325$ Pa is the atmospheric pressure and the speed of sound in this mixture is $\overline{c_b} = 862.3$ m/s. All quantities are represented using their time-averaged mean values with the notation $\overline{(\cdot)}$. A compact flame is taken to be stabilized in the combustion chamber dump plane. Assuming one-dimensional harmonic plane acoustic waves, the acoustic pressure and velocity in the jth section are[42]

$$p'_j(x,t) = A_j \exp\left[ik_j(x - x_j) - ist\right] + B_j \exp\left[-ik_j(x - x_j) - ist\right], \quad (5)$$

$$u'_j(x,t) = \frac{1}{\rho_j c_j}\left\{A_j \exp\left[ik_j(x - x_j) - ist\right] - B_j \exp\left[-ik_j(x - x_j) - ist\right]\right\}, \quad (6)$$

where A_j and B_j are the amplitudes, x_j is the interface position marked in Fig. 6, x is the axial position, t denotes time, $k_j = s/c_j$ is the acoustic

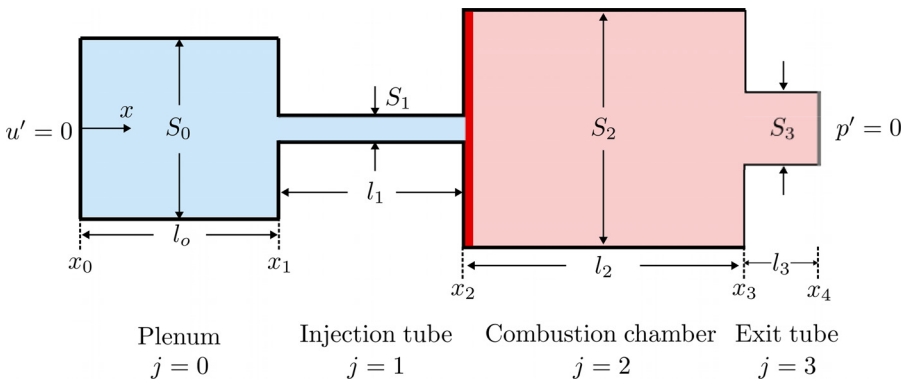

FIG. 6. Schematic of the 3-cavity acoustic model.

09 April 2025 06:56:50

© Author(s) 2025

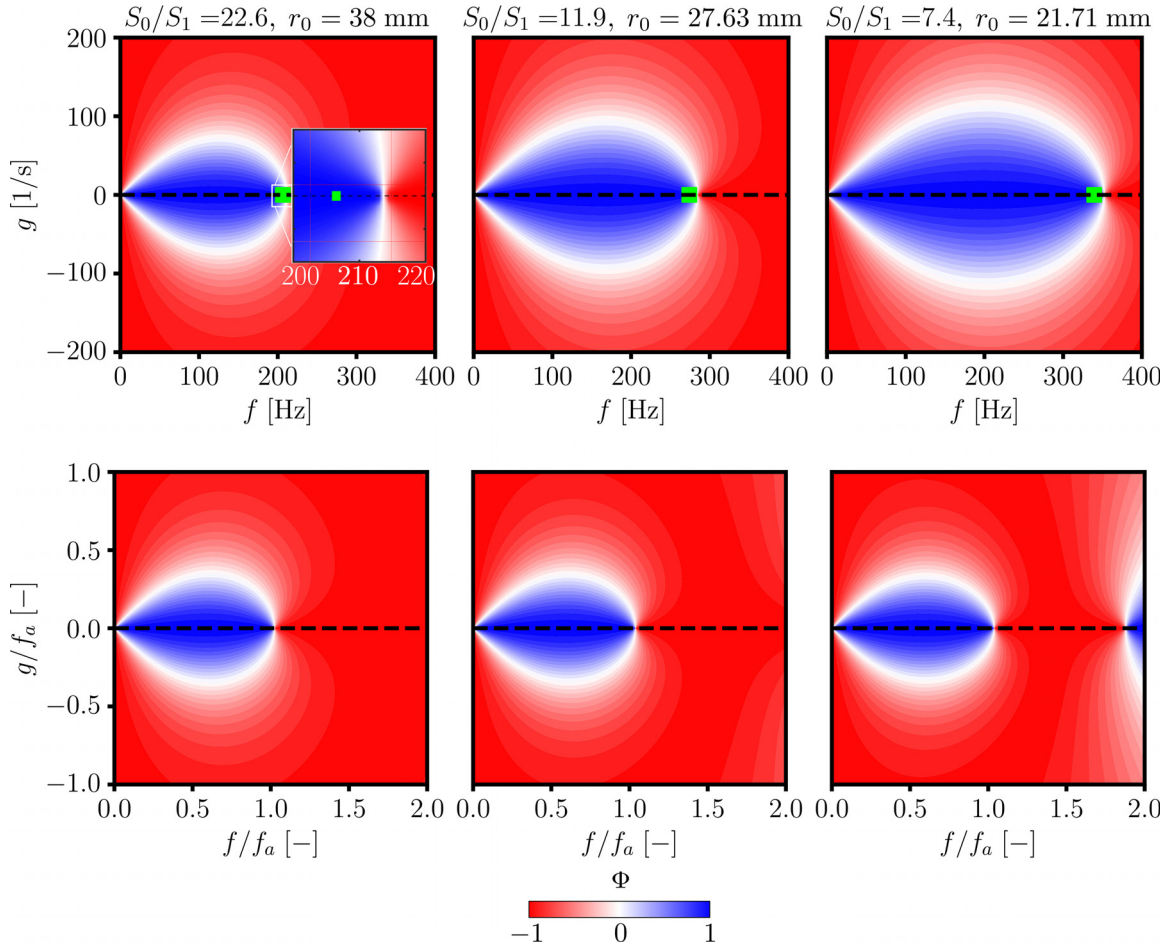

FIG. 7. Contour maps of Φ in the un-normalized (top row) and normalized (bottom row) eigenspace for three values of r_0 with a constant $r_1 = 8$ mm. The pure acoustic mode (for $\dot{Q}' = 0$) frequency, f_a, is marked using a green star. The blue regions correspond to acoustic modes, and red regions correspond to ITA modes. The pure acoustic mode frequencies are $f_a = 206.5$, 274 and 339.5 Hz for $r_0 = 38$, 27.63 and 21.71 mm, respectively.

wavenumber, $s = 2\pi(f - ig)$ is the eigenfrequency similar to Sec. II, and ρ_j and c_j are the density and speed of sound, respectively, for the gas mixture in the jth section. The length of each section is $l_j = x_{j+1} - x_j$, where $l_0 = 94$ mm, $l_1 = 30$ mm, $l_2 = 114$ mm, and $l_3 = 50 + 0.6r_3$ mm, considering an end correction of $0.6r_3$.[43] Moreover, $c_0 = c_1 = \overline{c_u}$, $\rho_0 = \rho_1 = \overline{\rho_u}$ and $k_0 = k_1 = k_u = \omega/\overline{c_u}$, whereas $c_2 = c_3 = \overline{c_b}$, $\rho_2 = \rho_3 = \overline{\rho_b}$ and $k_2 = k_3 = k_b = \omega/\overline{c_b}$.

The dispersion relation for this acoustic model is derived in Appendix A following Refs. 44 and 45. The focus here is on evaluating the phasor criterion that distinguishes between ITA and acoustic mode in the 3-cavity model. Rewriting Eq. (A10) in terms of u_1', u_2', Ξ, and β gives

$$S_1 \beta u_1' = S_2 u_2', \tag{7}$$

where $\beta = 1 + \mathscr{F}\Theta$, $\mathscr{F}$ is the flame transfer function and $\Theta = \overline{T_b}/\overline{T_u} - 1$. According to the phasor criterion, an acoustic mode satisfies $0 < \Phi \leq 1$ and an ITA mode satisfies $-1 \leq \Phi \leq 0$, where

$$\Phi = \cos\left[\angle\left(u_1', u_2'\right)\right] = \cos[\angle((S_1/S_2)\beta)]. \tag{8}$$

Rearranging the dispersion relation in Eq. (A12) gives β as

$$\beta = -\frac{K_3 \cos(k_b l_2) + K_4 \sin(k_b l_2)}{\Xi(K_1 + K_2)}, \tag{9}$$

where K_1, K_2, K_3, and K_4 are given in Eq. (A13).

The quantity Φ can be evaluated directly using Eqs. (8) and (9) by sweeping across the entire eigenspace without the need for computationally expensive iterative solutions of dispersion relations. The validation of the ansatz against Yong *et al.*[18] results for a 2-cavity model is provided in Appendix B. The effect of the area ratio on Φ, not explored by Yong *et al.*,[18] is also presented in Appendix B. This section discusses the effects of the area ratio on Φ and the eigenspectrum for a 3-cavity model, focusing solely on the impact of S_0/S_1 on the plenum mode. Contour maps of Φ evaluated using Eqs. (8) and (9) for three values of r_0 with a constant $r_1 = 8$ mm are shown in Fig. 7. The blue and red regions correspond to the acoustic $(0 < \Phi \leq 1)$ and ITA $(-1 \leq \Phi \leq 0)$ modes, respectively. An analogy between these modes and the two modes of oscillation in a coupled pendula is discussed in the supplementary material. The top row of Fig. 7 shows that as r_0

09 April 2025 06:56:50

© Author(s) 2025

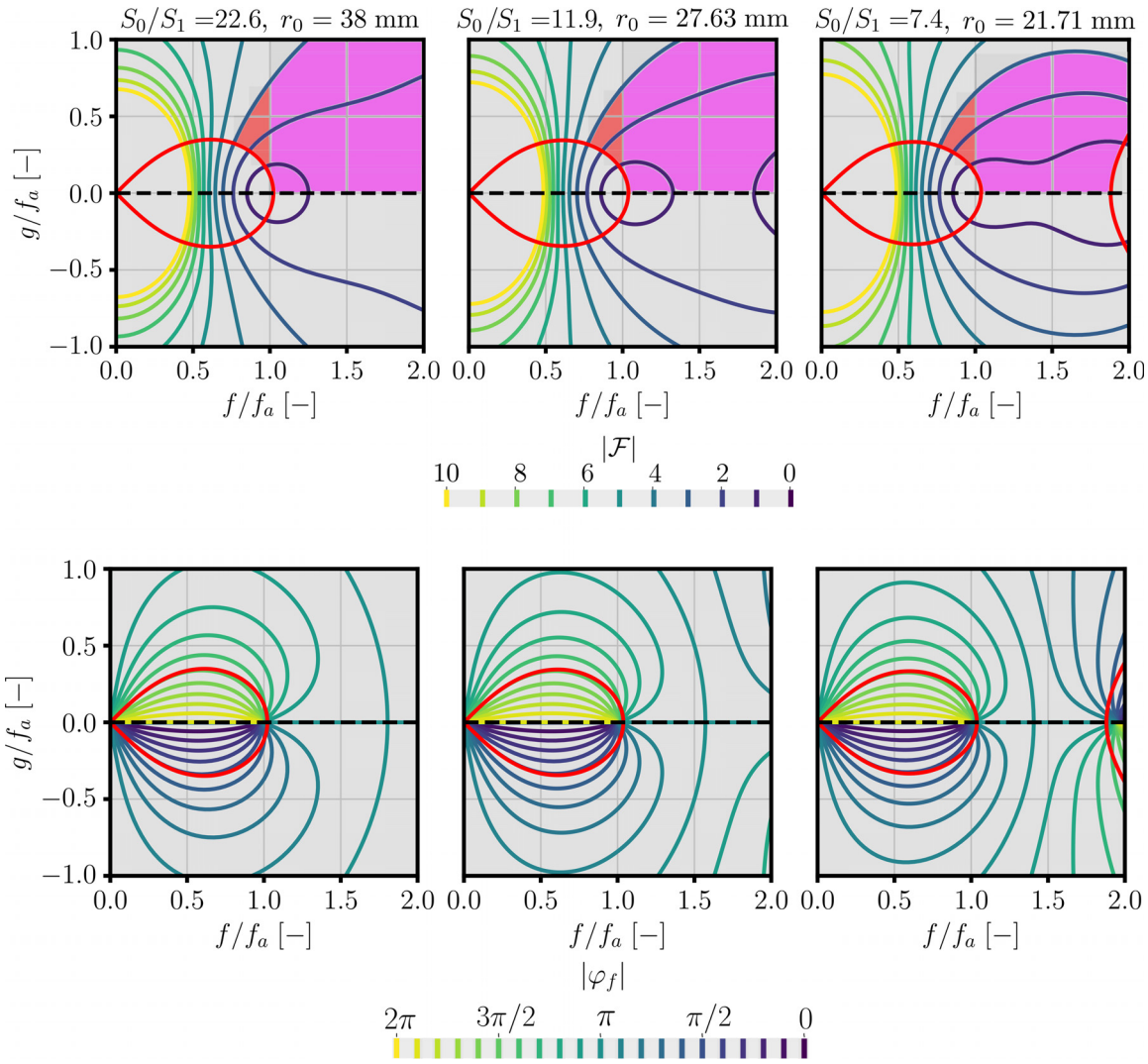

FIG. 8. Contours of $|\mathscr{F}|$ (top row) and φ_f (bottom row) in the eigenspace for three values of r_0 with a constant $r_1 = 8$ mm. The red contour marks $\Phi = 0$, separating ITA modes ($\Phi < 0$) outside the contour from acoustic modes ($\Phi > 0$) inside it. The pink and red shaded regions mark the unstable ITA modes for $|\mathscr{F}| < 3$ when $f/f_a > 1$ and $f/f_a < 1$, respectively.

decreases, the size of the acoustic region ($\Phi > 0$) increases, implying that unstable ITA modes ($\Phi < 0$) appear at higher frequencies or growth rates. At the pure acoustic mode frequency f_a, the plenum and injection tube act like a Helmholtz resonator with a frequency proportional to $\sqrt{S_1/S_0}$. Consequently, the Φ contours around the plenum mode are invariant to changes in S_0 when normalized by f_a (see Fig. 7, bottom row). The blue region seen in the normalized Φ contour plot for $r_0 = 21.71$ mm close to $f/f_a = 2.0$ is related to the chamber mode and will not be discussed further.

The contours of the flame gain $|\mathscr{F}|$ and phase φ_f for three values of r_0 with a constant $r_1 = 8$ mm are shown in Fig. 8. Intrinsic modes are stabilized by decreasing r_0 as seen by the shrinking of the pink region marking ITA modes for $f/f_a > 1$ and a flame gain lower than 3, typically observed in this burner.[4,15]

Intrinsic modes with physically realizable gain ($|\mathscr{F}| < 3$) appear in a narrow region marked in red, which remain unaffected to changes in the plenum radius. The bottom row of Fig. 8 shows that phase contours become more compact upon increasing r_0. Intrinsic modes occur in the interval $\pi/2 \leq \varphi_f \leq 3\pi/2$ and become unstable for $\pi \leq \varphi_f \leq 3\pi/2$. Moving outward from the $\Phi = 0$ contour into the unstable region, the flame phase decreases, reducing time delays. Thus, reductions in time delay, such as those caused by H_2 addition,[4,5,20] destabilize intrinsic modes.

Figure 9 shows the flame gain and phase contours for three values of r_1 with a constant $r_0 = 38$ mm. In contrast to Fig. 8, increasing r_1 (or decreasing S_0/S_1) increases the size of the red-shaded region, indicating that unstable ITA modes become more prominent for $f/f_a < 1$. Intrinsic modes are more sensitively stabilized by reducing r_1 than r_0,

09 April 2025 06:56:50

© Author(s) 2025

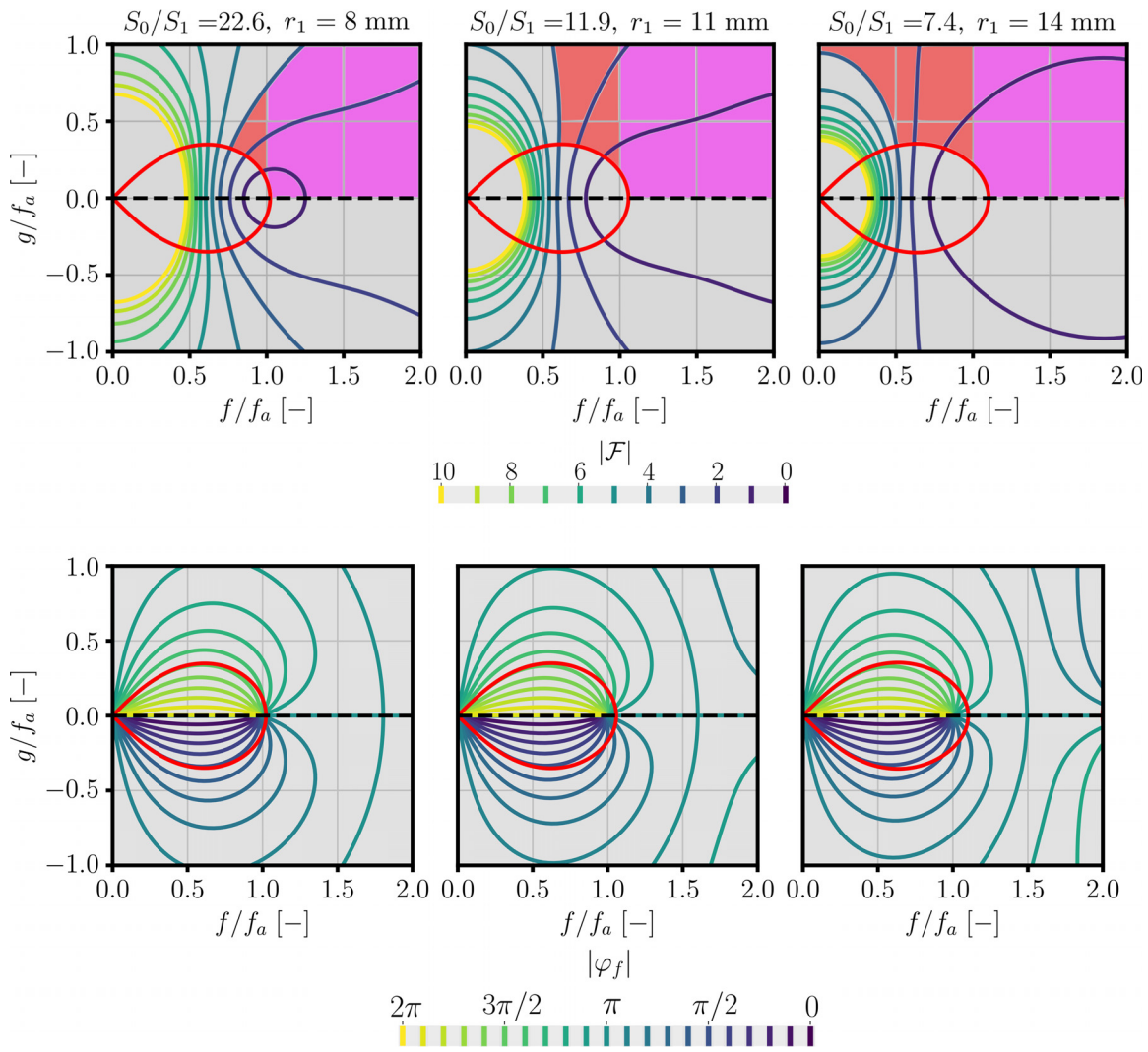

FIG. 9. Same as in Fig. 8 for three values of r_1 with a constant $r_0 = 38$ mm.

as shown by the shrinking pink-shaded region. The φ_f contours follow a similar trend to those observed when r_0 was varied.

These results are in contrast with Mukherjee and Shrira,[46] who found that intrinsic modes with a small interaction index n are geometry-independent. However, in this study, frequency and growth rates of ITA modes identified by the phasor criterion depend on geometric parameters like S_0/S_1. Additionally, these results further extend those of Yong *et al.*[18] to multiple cavity systems with non-unity area ratios. Unlike the results of Schuller *et al.*,[47] it is shown in this study that ITA modes can be destabilized even in combustors with moderate confinement and flame gain.

The geometrical parameters of the 3-cavity model closely approximate those of the PRECCINSTA burner, with S_0/S_1 expected to range between 7.4 and 11.9. Precisely determining these values is challenging due to the burner's non-uniform duct areas, but this provides a good first approximation. For instance, at the EP, the ROM yields $\tau_{EP} \approx 1.223$ ms and $n_{EP} \approx 0.361$, while the 3-cavity acoustic model gives $1.3015 > \tau_{EP} > 1.1162$ ms and $0.2636 < n_{EP} < 0.4081$ for $11.9 > S_0/S_1 > 7.4$. Thus, both τ_{EP} and n_{EP} fall within the expected range.

Despite these limitations, the 3-cavity model reveals useful insights while a more accurate ROM can be employed for quantitative accuracy. It was shown using the 3-cavity model that ITA modes, identified using the phasor criterion, can be stabilized by reducing the cross-sectional area of either the plenum or the injection tube, with greater sensitivity to the latter. Furthermore, for large injection tube cross-sectional areas, ITA modes with moderate gain ($|\mathcal{F}| < 3$) are present in regions where $f/f_a \leq 1$. Thus, ITA modes should not be ruled out for limit-cycle oscillations at $f \approx f_a$. Moreover, the non-iterative procedure used for this study circumvents the tedious evaluation of the dispersion relation, reducing the computational cost and accelerating the early stages of stable combustor design.

09 April 2025 06:56:50

© Author(s) 2025

V. CONCLUSIONS

The effects of hydrogen addition on thermoacoustic instabilities are investigated in a partially premixed swirl combustor. An intrinsic thermoacoustic feedback loop corresponding to a plenum mode is identified in the PRECCINSTA burner using the phasor criterion.[18] Intrinsic modes are evidenced by (i) the large deviation of the thermoacoustic instability frequency from the cavity acoustic modes and (ii) the change in the axial pressure gradient across the flame, which is captured in LES and further substantiated by an ROM. The eigenspectrum of the combustor reveals the emergence of intrinsic modes as the time lag τ decreases and the interaction index n increases. The time lag decreases and the interaction index increases with the addition of H_2, at least for the cases investigated here, and hence ITA modes ensue. This observation is different from the stabilizing effect of H_2 addition on the ITA modes observed previously.[20] This is largely because of the reduction in the flame gain in,[20] whereas the gain increases with the H_2 addition in the present study. Therefore, making general conclusions regarding the effects of H_2 on thermoacoustic stability is challenging, and more experimental, theoretical, and numerical investigations are required.

A 1D acoustic model is used to obtain additional insight that is not specific to the PRECCINSTA burner used for LES and experiments. It is shown that ITA modes can be stabilized by reducing the cross-sectional areas of the plenum or the injection tube, with greater sensitivity to the latter. For large injection tube areas, unstable ITA modes can also be found near the passive acoustic mode frequency. Thus, ITA modes should not be ruled out for limit-cycle oscillations near this frequency. The 1D acoustic model provides a useful guide to avoid regions of both classical and intrinsic instabilities during a combustor design. Its non-iterative evaluation of dispersion relations offers quick stability estimates, which can inform more accurate quantitative assessments using ROM in the early design phase.

SUPPLEMENTARY MATERIAL

See the supplementary material contains an analogy of the coupled pendula and the effect of flame position.

ACKNOWLEDGMENTS

A.D.K. acknowledges financial support from the Cambridge Trust and from the Cambridge Philosophical Society through a Henslow Junior Research Fellowship at Robinson College, University of Cambridge. A.D.K, J.C.M, and N.S. acknowledge the support from MHI, Ltd., Takasago, Japan. This work used the ARCHER2 UK National Supercomputing Service (https://www.archer2.ac.uk). The EPSRC (Grant No. EP/R029369/1) and ARCHER2 are acknowledged for financial and computational support as a part of their funding to the UK Consortium on Turbulent Reacting Flows (https://www.ukctrf.com). P.R.S. acknowledges the funding from the Horizon Europe research and Innovation program HESTIA under Grant Agreement No. 101056865. The measurements were made using funding from the European Research Council (ERC) under the EU Horizon 2020 research and innovation programme (Grant Agreement No.682383).

AUTHOR DECLARATIONS

Conflict of Interest

The authors have no conflicts to disclose.

Author Contributions

Ankit D. Kumar: Conceptualization (lead); Data curation (lead); Formal analysis (lead); Investigation (lead); Methodology (lead); Software (lead); Validation (lead); Visualization (lead); Writing – original draft (lead); Writing – review & editing (lead). **James C. Massey:** Methodology (lead); Software (equal); Supervision (supporting); Writing – review & editing (equal). **Preethi Rajendram Soundararajan:** Investigation (equal); Methodology (equal); Software (equal); Writing – review & editing (equal). **Isaac Boxx:** Funding acquisition (equal); Project administration (supporting); Resources (supporting); Writing – review & editing (equal). **Nedunchezhian Swaminathan:** Conceptualization (supporting); Investigation (supporting); Methodology (supporting); Project administration (equal); Resources (equal); Supervision (lead); Writing – review & editing (equal).

DATA AVAILABILITY

The data that support the findings of this study are available from the corresponding author upon reasonable request.

APPENDIX A: DERIVATION OF THE 3-CAVITY ACOUSTIC MODEL

Equations (5) and (6) satisfy the standard acoustic jump conditions at the interfaces between sections. For the sake of simplicity, the inlet and outlet boundaries are assumed to be closed ($u' = 0$) and open ($p' = 0$), respectively, which gives the following set of equations while considering only spatial variation:

$$u_0'(0) = 0 \Rightarrow A_0 - B_0 = 0 \tag{A1}$$

$$p_0'(l_0) = p_1'(l_0) \Rightarrow A_0 e^{ik_u l_0} + B_0 e^{-ik_u l_0} - A_1 - B_1 = 0 \tag{A2}$$

$$S_0 u_0'(l_0) = S_1 u_1'(l_0) \Rightarrow \frac{S_0}{\overline{\rho_u}\,\overline{c_u}}\left[A_0 e^{ik_u l_0} - B_0 e^{-ik_u l_0}\right] - \frac{S_1}{\overline{\rho_u}\,\overline{c_u}}\left[A_1 - B_1\right] = 0 \tag{A3}$$

$$p_1'(l_0 + l_1) = p_2'(l_0 + l_1) \Rightarrow A_1 e^{ik_u l_1} + B_1 e^{-ik_u l_1} - A_2 - B_2 = 0 \tag{A4}$$

$$S_1 u_1'(l_0 + l_1) + \frac{\gamma - 1}{\overline{\rho_u}\,\overline{c_u}^2}\dot{Q}' = S_2 u_2'(l_0 + l_1) \Rightarrow \frac{S_1}{\overline{\rho_u}\,\overline{c_u}}\left[A_1 e^{ik_u l_1} - B_1 e^{-ik_u l_1}\right] + \frac{\gamma - 1}{\overline{\rho_u}\,\overline{c_u}^2}\dot{Q}' - \frac{S_2}{\overline{\rho_b}\,\overline{c_b}}\left[A_2 - B_2\right] = 0 \tag{A5}$$

$$p_2'(l_0 + l_1 + l_2) = p_3'(l_0 + l_1 + l_2) \Rightarrow A_2 e^{ik_b l_2} + B_2 e^{-ik_b l_2} - A_3 - B_3 = 0 \tag{A6}$$

$$S_2 u_2'(l_0 + l_1 + l_2) = S_3 u_3'(l_0 + l_1 + l_2) \Rightarrow \frac{S_2}{\overline{\rho_b}\,\overline{c_b}}\left[A_2 e^{ik_b l_2} - B_2 e^{-ik_b l_2}\right] - \frac{S_3}{\overline{\rho_b}\,\overline{c_b}}\left[A_3 - B_3\right] = 0 \tag{A7}$$

$$p_3'(l_0 + l_1 + l_2 + l_3) = 0 \Rightarrow A_3 e^{ik_b l_3} + B_3 e^{-ik_b l_3} = 0. \tag{A8}$$

09 April 2025 06:56:50

© Author(s) 2025

Fluctuations are denoted as $(\cdot)' = (\cdot) - \overline{(\cdot)}$, where the overbar denotes time-averaging. The Fourier-transformed heat release rate perturbations, $\dot{Q}$, can be expressed in terms of Fourier-transformed velocity perturbations using either a Flame Describing Function (FDF) or Flame Transfer Function (FTF), which takes the following generic form:

$$\mathscr{F} = |\mathscr{F}|e^{i\varphi_f} = \frac{\hat{\dot{Q}}/\overline{\dot{Q}}}{\hat{u}_1/\overline{u_1}}, \tag{A9}$$

where $|\mathscr{F}|$ and φ_f are the gain and phase of the FTF/FDF, respectively, $\overline{\dot{Q}}$ is the time-averaged heat release rate, $\overline{u}_1$ is the time-averaged velocity at the base of the flame. The flame is assumed to be at the dump plane such that $l_f = 0$ mm. The interested reader can refer to the supplementary material for the effects of the flame position, which are found to be negligible around the plenum mode. The time-averaged heat release rate is expressed as $\overline{\dot{Q}} = \dot{m}\overline{C_p}(\overline{T_b} - \overline{T_u})$, where $\dot{m} = \overline{\rho_u} S_1 \overline{u}_1$ is the total mass flow rate and $\overline{C_p}$ is the specific heat capacity at a constant pressure. Using perfect gas relations and $\overline{c_u}^2 = \gamma R \overline{T_u}$, Eq. (A5) can be rewritten as

$$\frac{S_1}{\overline{\rho_u}\,\overline{c_u}}\underbrace{(1+\mathscr{F}\Theta)}_{\beta}\left[A_1 e^{ik_u l_1} - B_1 e^{-ik_u l_1}\right] - \frac{S_2}{\overline{\rho_b}\,\overline{c_b}}\left[A_2 - B_2\right] = 0, \tag{A10}$$

where $\Theta = (\overline{T_b}/\overline{T_u} - 1)$. Equations (A1)–(A4), (A6)–(A8) and (A10) form a set of linear equations that can be expressed in a matrix form as $\mathbf{MX} = 0$, where $\mathbf{X} = [A_0\ B_0\ A_1\ B_1\ A_2\ B_2\ A_3\ B_3]^\top$ and $\mathbf{M}$ is

$$\begin{bmatrix}
1 & -1 & 0 & 0 & 0 & 0 & 0 & 0 \\
e^{ik_u l_0} & e^{-ik_u l_o} & -1 & -1 & 0 & 0 & 0 & 0 \\
\frac{S_0}{\overline{\rho_u}\,\overline{c_u}}e^{ik_u l_0} & -\frac{S_0}{\overline{\rho_u}\,\overline{c_u}}e^{-ik_u l_0} & -\frac{S_1}{\overline{\rho_u}\,\overline{c_u}} & \frac{S_1}{\overline{\rho_u}\,\overline{c_u}} & 0 & 0 & 0 & 0 \\
0 & e^{ik_u l_1} & e^{-ik_u l_1} & -1 & -1 & 0 & 0 & 0 \\
0 & 0 & \Xi\beta e^{ik_u l_1} & -\Xi\beta e^{-ik_u l_1} & -1 & 1 & 0 & 0 \\
0 & 0 & 0 & 0 & e^{ik_b l_2} & e^{-ik_b l_2} & -1 & -1 \\
0 & 0 & 0 & 0 & S_2 e^{ik_b l_2} & -S_2 e^{-ik_b l_2} & -S_3 & S_3 \\
0 & 0 & 0 & 0 & 0 & 0 & e^{ik_b l_3} & e^{-ik_b l_3}
\end{bmatrix}, \tag{A11}$$

where $\Xi = (S_1/S_2)(\overline{\rho_b}\,\overline{c_b}/\overline{\rho_u}\,\overline{c_u})$. Non-trivial solutions satisfy $\det[\mathbf{M}] = 0$. The quantity $\Xi\beta$ denotes the coupling index. In a past study,[45] such a coupling was considered in the absence of flame dynamics, which is condensed here into β. The determinant of matrix $\mathbf{M}$ gives the following dispersion relation:

$$(K_1 + K_2)\Xi\beta + K_3\cos(k_b l_2) + K_4\sin(k_b l_2) = 0, \tag{A12}$$

where K_1, K_2, K_3, and K_4 are given by

$$\begin{aligned}
K_1 &\equiv S_2\cos(k_b l_2)\sin(k_b l_3) \\
&\quad [\sin(k_u l_0)S_0\cos(k_u l_1) + \sin(k_u l_1)\cos(k_u l_0)S_1] \\
K_2 &\equiv S_3\cos(k_b l_3)\sin(k_b l_2) \\
&\quad [\sin(k_u l_0)S_0\cos(k_u l_1) + \sin(k_u l_1)\cos(k_u l_0)S_1] \\
K_3 &\equiv -S_3\cos(k_b l_3) \\
&\quad [\cos(k_u l_0)\cos(k_u l_1)S_1 - \sin(k_u l_0)\sin(k_u l_1)S_0] \\
K_4 &\equiv S_2\sin(k_b l_3) \\
&\quad [\cos(k_u l_0)\cos(k_u l_1)S_1 - \sin(k_u l_0)\sin(k_u l_1)S_0]
\end{aligned} \tag{A13}$$

APPENDIX B: 2-CAVITY MODEL

The dispersion relation for a two-cavity model shown in (Fig. 10) is given by

$$\zeta\frac{S_1}{S_0}\cos(kl_0)\cos(kl_1) - \underbrace{(1+\mathscr{F}\Theta)}_{\beta}\sin(kl_0)\sin(kl_1) = 0, \tag{B1}$$

where $\zeta = \overline{\rho}_u\,\overline{c_u}/\overline{\rho_b}\,\overline{c_b}$. Equation (B1) is similar to the dispersion relation presented by Yong *et al.*[17] except that in that study $S_1/S_0 = 1$. The phasor depends on $(S_0/S_1)\beta$ as $\Phi = \cos[\angle((S_0/S_1)\beta)]$ [similar to Eq. (6)], which for a two-cavity model can be obtained by rearranging Eq. (B1)

$$\frac{S_0}{S_1}\beta = \zeta\cot(kl_0)\cot(kl_1). \tag{B2}$$

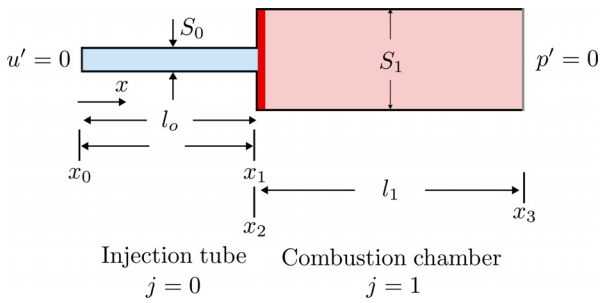

FIG. 10. Schematic of the 2-cavity acoustic model.

09 April 2025 06:56:50

© Author(s) 2025

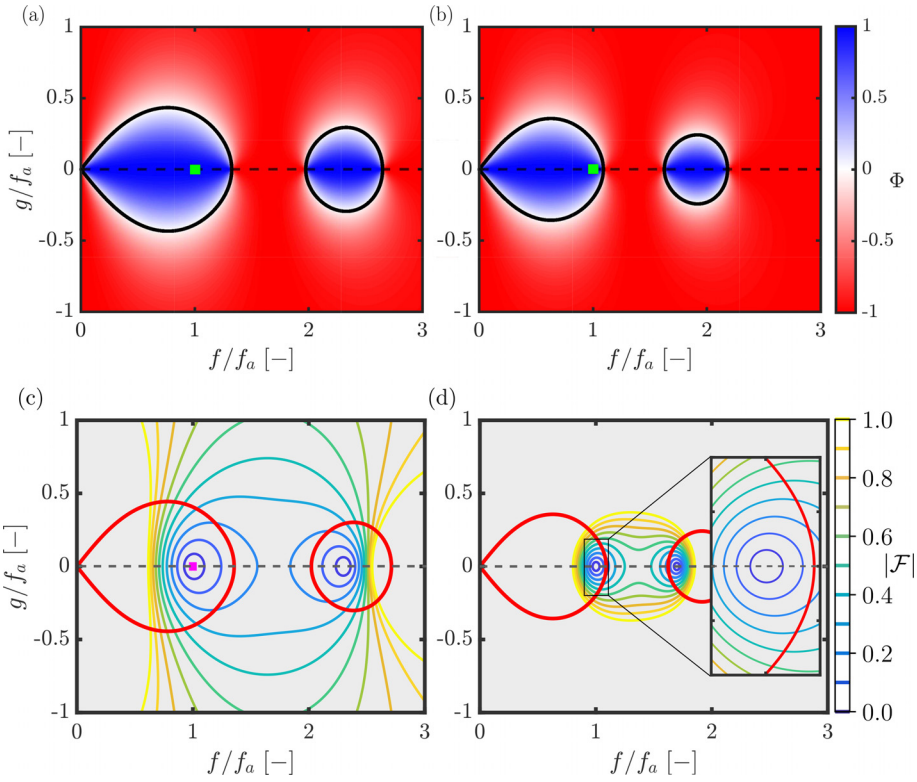

FIG 11. Contours of Φ (a) and (b) and $|\mathscr{F}|$ (c,d) for an ideal resonator with (a) and (c) $S_1/S_0 = 1$ and identical to Fig. 13 in Ref. 18 and (b,d) $S_1/S_0 = 5$. The black contour line corresponds to $\Phi = 0$. The green and pink squares mark the pure acoustic mode $f = f_a$.

Contours of Φ are shown in Figs. 11(a) and 11(b) for $S_1/S_0 = 1$ and $S_1/S_0 = 5$. The results for S_1/S_0 are identical to Fig. 13 of Ref. 18 with $l_0 = 0.36$ m and $l_1 = 0.54$ m. All other parameters are the same as in Table II in that work. The size of the acoustic mode region (in blue) decreases as S_1/S_0 increases. However, the Φ contours are independent of S_1/S_0 in the unnormalized eigenspace (not shown). It can also be seen from Figs. 11(a) and 11(b) that the pure acoustic mode approaches the $\Phi = 0$ contour line as S_1/S_0 increases. The pure acoustic mode cannot lie on the $\Phi = 0$ line. This is straightforward to understand from the equation for the dot product of u_0' and u_1' given by

$$u_0' \cdot u_1' = |u_0'|^2 \left(\frac{S_0}{S_1}\right)\left(1 + \theta|\mathscr{F}|\cos(\varphi_f)\right). \tag{B3}$$

The above equation is easily derived from the velocity jump condition at the area jump and the definition of the flame transfer function $\mathscr{F}$. This equation is similar to Eq. (36) of Yong *et al.*[18] and differs only by the area ratio S_0/S_1, which was equal to unity in that study. For the pure acoustic mode $|\mathscr{F}| = 0$ (i.e., no flame), therefore $u_0' \cdot u_1' = |u_0'|^2(S_0/S_1) \neq 0$. Since $\Phi = \cos(\angle(u_0', u_1')) = (u_0' \cdot u_1')/(|u_0'||u_0'|)$ for the 2-cavity model, it cannot be equal to zero when $|\mathscr{F}| = 0$. In other words, the pure acoustic mode cannot coincide with the location of $\Phi = 0$. While the pure acoustic mode approaches the $\Phi = 0$ contour line, it will never coincide with the $\Phi = 0$ contour line. This is clearly shown in Fig. 11(d), which shows the contours of $|\mathscr{F}|$ along with the $\Phi = 0$ contour line. It can be seen that the contours of $|\mathscr{F}|$ become more closely spaced as S_1/S_0 increases. Furthermore, the inset in Fig. 11(d) shows that the pure acoustic mode is not coinciding with the $\Phi = 0$ contour line and that the $|\mathscr{F}|$ takes finite non-zero values on this contour line. The pure acoustic mode coincides with the $\Phi = 0$ contour line only as $S_0/S_1 \to 0$ as seen from Eq. (B3).

REFERENCES

[1] T. C. Lieuwen and V. Yang, *Combustion Instabilities In Gas Turbine Engines: Operational Experience, Fundamental Mechanisms, and Modeling* (American Institute of Aeronautics and Astronautics, 2006), Vol. 144, pp. 360–369.

[2] A. Datta, S. Gupta, I. Chterev, I. Boxx, and S. Hemchandra, "Impact of hydrogen addition on the thermoacoustic instability and precessing vortex core dynamics in a CH4/H2/air technically premixed combustor," J. Eng. Gas Turb. Power **144**, 021013 (2022).

[3] P. W. Agostinelli, D. Laera, I. Chterev, I. Boxx, L. Gicquel, and T. Poinsot, "On the impact of H2-enrichment on flame structure and combustion dynamics of a lean partially-premixed turbulent swirling flame," Combust. Flame. **241**, 112120 (2022).

[4] A. M. Garcia, S. Le Bras, J. Prager, I. Boxx, and W. Polifke, "Impact of H2-enrichment on the response of a partially premixed CH4–air flame to velocity and equivalence ratio fluctuations," Combust. Flame **268**, 113595 (2024).

[5] A. D. Kumar, J. C. Massey, I. Boxx, and N. Swaminathan, "Effects of hydrogen enrichment on thermoacoustic and helical instabilities in swirl stabilised partially premixed flames," Flow. Turbul. Combust. **112**, 689–727 (2024).

[6] M. Hoeijmakers, V. Kornilov, I. L. Arteaga, P. de Goey, and H. Nijmeijer, "Intrinsic instability of flame–acoustic coupling," Combust. Flame **161**, 2860–2867 (2014).

[7] C. F. Silva, T. Emmert, S. Jaensch, and W. Polifke, "Numerical study on intrinsic thermoacoustic instability of a laminar premixed flame," Combust. Flame **162**, 3370–3378 (2015).

[8] E. Courtine, L. Selle, and T. Poinsot, "DNS of intrinsic thermoacoustic modes in laminar premixed flames," Combust. Flame **162**, 4331–4341 (2015).

09 April 2025 06:56:50

© Author(s) 2025

[9]C. F. Silva, "Intrinsic thermoacoustic instabilities," Prog. Energy Combust. Sci. **95**, 101065 (2023).
[10]T. Emmert, S. Bomberg, S. Jaensch, and W. Polifke, "Acoustic and intrinsic thermoacoustic modes of a premixed combustor," Proc. Combust. Inst. **36**, 3835–3842 (2017).
[11]D. Fredrich, W. P. Jones, and A. J. Marquis, "Thermo-acoustic instabilities in the PRECCINSTA combustor investigated using a compressible LES-PDF approach," Flow. Turbul. Combust. **106**, 1399–1415 (2021).
[12]P. W. Agostinelli, D. Laera, I. Boxx, L. Gicquel, and T. Poinsot, "Impact of wall heat transfer in large eddy simulation of flame dynamics in a swirled combustion chamber," Combust. Flame **234**, 111728 (2021).
[13]B. Franzelli, E. Riber, L. Y. Gicquel, and T. Poinsot, "Large eddy simulation of combustion instabilities in a lean partially premixed swirled flame," Combust. Flame **159**, 621–637 (2012).
[14]J.-M. Lourier, M. Stöhr, B. Noll, S. Werner, and A. Fiolitakis, "Scale adaptive simulation of a thermoacoustic instability in a partially premixed lean swirl combustor," Combust. Flame **183**, 343–357 (2017).
[15]J. Kuhlmann, S. Marragou, I. Boxx, T. Schuller, and W. Polifke, "LES-based prediction of technically premixed flame dynamics and comparison with perfectly premixed mode," Phys. Fluids **34**, 085125 (2022).
[16]L. Xu, J. Zheng, G. Wang, Z. Feng, X. Tian, L. Li, and F. Qi, "Investigation on the intrinsic thermoacoustic instability of a lean-premixed swirl combustor with an acoustic liner," Proc. Combust. Inst. **38**, 6095–6103 (2021).
[17]K. J. Yong, C. F. Silva, and W. Polifke, "A categorization of marginally stable thermoacoustic modes based on phasor diagrams," Combust. Flame **228**, 236–249 (2021).
[18]K. J. Yong, C. F. Silva, G. J. Fournier, and W. Polifke, "Categorization of thermoacoustic modes in an ideal resonator with phasor diagrams," Combust. Flame **249**, 112605 (2023).
[19]A. Albayrak, T. Steinbacher, T. Komarek, and W. Polifke, "Convective scaling of intrinsic thermo-acoustic eigenfrequencies of a premixed swirl combustor," J. Eng. Gas Turbines Power **140**, 041510 (2018).
[20]A. Ghani andW. Polifke, "Control of intrinsic thermoacoustic instabilities using hydrogen fuel," Proc. Combust. Inst. **38**, 6077–6084 (2021).
[21]L. Crocco, "Theoretical studies on liquid-propellant rocket instability," Proc. Combust. Inst. **10**, 1101–1128 (1965).
[22]A. Orchini, C. F. Silva, G. A. Mensah, and J. P. Moeck, "Thermoacoustic modes of intrinsic and acoustic origin and their interplay with exceptional points," Combust. Flame **211**, 83–95 (2020).
[23]T. Emmert, S. Bomberg, and W. Polifke, "Intrinsic thermoacoustic instability of premixed flames," Combust. Flame **162**, 75–85 (2015).
[24]N. Hosseini, V. Kornilov, I. Lopez Arteaga, W. Polifke, O. Teerling, and L. de Goey, "Intrinsic thermoacoustic modes and their interplay with acoustic modes in a Rijke burner," Int. J. Spray Combust. **10**, 315–325 (2018).
[25]S. Ruan, N. Swaminathan, and O. Darbyshire, "Modelling of turbulent lifted jet flames using flamelets: A priori assessment and a posteriori validation," Combust. Theory Model. **18**, 295–329 (2014).
[26]Z. Chen, S. Ruan, and N. Swaminathan, "Large Eddy Simulation of flame edge evolution in a spark-ignited methane-air jet," Proc. Combust. Inst. **36**, 1645–1652 (2017).
[27]J. C. Massey, Z. X. Chen, M. Stöhr, W. Meier, and N. Swaminathan, "On the blow-off correlation for swirl-stabilised flames with a precessing vortex core," Combust. Flame **239**, 111741 (2022).
[28]R. W. Bilger, "The structure of turbulent nonpremixed flames," Proc. Combust. Inst. **22**, 475–488 (1989).
[29]A. D. Kumar, J. C. Massey, M. Stöhr, W. Meier, and N. Swaminathan, "Period-2 thermoacoustics in a swirl-stabilised partially premixed flame computed using large eddy simulation," Flow. Turbul. Combust. **111**, 995–1028 (2023).
[30]W. Meier, P. Weigand, X. R. Duan, and R. Giezendanner-Thoben, "Detailed characterization of the dynamics of thermoacoustic pulsations in a lean premixed swirl flame," Combust. Flame. **150**, 2–26 (2007).
[31]Z. X. Chen and N. Swaminathan, "Influence of fuel plenum on thermoacoustic oscillations inside a swirl combustor," Fuel **275**, 117868 (2020).
[32]C. Kraus, L. Selle, and T. Poinsot, "Coupling heat transfer and large eddy simulation for combustion instability prediction in a swirl burner," Combust. Flame **191**, 239–251 (2018).
[33]Y. Gong, "Applications of a numerical method in study of combustion instabilities," Ph.D. thesis (Imperial College London, 2022).
[34]W.-J. Beyn, "An integral method for solving nonlinear eigenvalue problems," Linear Algebra Appl. **436**, 3839–3863 (2012).
[35]A. Ghani, T. Steinbacher, A. Albayrak, and W. Polifke, "Intrinsic thermoacoustic feedback loop in turbulent spray flames," Combust. Flame **205**, 22–32 (2019).
[36]M. Merk, S. Jaensch, C. Silva, and W. Polifke, "Simultaneous identification of transfer functions and combustion noise of a turbulent flame," J. Sound Vib. **422**, 432–452 (2018).
[37]A. J. Eder, C. F. Silva, M. Haeringer, J. Kuhlmann, and W. Polifke, "Incompressible versus compressible large eddy simulation for the identification of premixed flame dynamics," Int. J. Spray Combust. **15**, 16–32 (2023).
[38]C. E. Martin, L. Benoit, Y. Sommerer, F. Nicoud, and T. Poinsot, "Large-eddy simulation and acoustic analysis of a swirled staged turbulent combustor," AIAA J. **44**, 741–750 (2006).
[39]P. Rajendram Soundararajan, G. Vignat, D. Durox, A. Renaud, and S. Candel, "Do flame describing functions suitably represent combustion dynamics under self-sustained oscillations?," J. Sound Vib. **534**, 117034 (2022).
[40]M. Murugesan, B. Singaravelu, A. K. Kushwaha, and S. Mariappan, "Onset of flame-intrinsic thermoacoustic instabilities in partially premixed turbulent combustors," Int. J. Spray Combust. **10**, 171–184 (2018).
[41]G. A. Mensah, L. Magri, C. F. Silva, P. E. Buschmann, and J. P. Moeck, "Exceptional points in the thermoacoustic spectrum," J. Sound Vib. **433**, 124–128 (2018).
[42]T. Poinsot and D. Veynante, *Theoretical and Numerical Combustion* (RT Edwards, Inc., 2005).
[43]S. W. Rienstra and A. Hirschberg, "An introduction to acoustics," "Report IWDE 92–06," (Technische Universiteit Eindhoven, 2004).
[44]P. Palies, D. Durox, T. Schuller, and S. Candel, "Nonlinear combustion instability analysis based on the flame describing function applied to turbulent premixed swirling flames," Combust. Flame **158**, 1980–1991 (2011).
[45]T. Schuller, D. Durox, P. Palies, and S. Candel, "Acoustic decoupling of longitudinal modes in generic combustion systems," Combust. Flame **159**, 1921–1931 (2012).
[46]N. K. Mukherjee and V. Shrira, "Intrinsic flame instabilities in combustors: Analytic description of a 1-D resonator model," Combust. Flame **185**, 188–209 (2017).
[47]T. Schuller, T. Poinsot, and S. Candel, "Dynamics and control of premixed combustion systems based on flame transfer and describing functions," J. Fluid Mech. **894**, P1 (2020).

09 April 2025 06:56:50

© Author(s) 2025